High-level cognition is supported by information-rich but compressible brain activity patterns

Lucy L. W. Owen^{a,b,c} and Jeremy R. Manning^{b,1}

Affiliations are included on p. 11.

Edited by Michael Breakspear, The University of Newcastle—Newcastle City Campus, Newcastle, NSW; received January 3, 2024; accepted July 8, 2024, by Editorial Board Member Michael S. Gazzaniga

To efficiently yet reliably represent and process information, our brains need to produce information-rich signals that differentiate between moments or cognitive states, while also being robust to noise or corruption. For many, though not all, natural systems, these two properties are often inversely related: More information-rich signals are less robust, and vice versa. Here, we examined how these properties change with ongoing cognitive demands. To this end, we applied dimensionality reduction algorithms and pattern classifiers to functional neuroimaging data collected as participants listened to a story, temporally scrambled versions of the story, or underwent a resting state scanning session. We considered two primary aspects of the neural data recorded in these different experimental conditions. First, we treated the maximum achievable decoding accuracy across participants as an indicator of the "informativeness" of the recorded patterns. Second, we treated the number of features (components) required to achieve a threshold decoding accuracy as a proxy for the "compressibility" of the neural patterns (where fewer components indicate greater compression). Overall, we found that the peak decoding accuracy (achievable without restricting the numbers of features) was highest in the intact (unscrambled) story listening condition. However, the number of features required to achieve comparable classification accuracy was also lowest in the intact story listening condition. Taken together, our work suggests that our brain networks flexibly reconfigure according to ongoing task demands and that the activity patterns associated with higher-order cognition and high engagement are both more informative and more compressible than the activity patterns associated with lower-order tasks and lower engagement.

information | compression | temporal decoding | dimensionality reduction | neuroimaging

Large-scale networks, including the human brain, may be conceptualized as occupying one or more positions along on a continuum. At one extreme, every node is fully independent from every other node. At the other extreme, all nodes behave identically. Each extreme optimizes key properties of how the network functions. When every node is independent, the network is maximally expressive: If we define the network's "state" as the activity pattern across its nodes, then every state is equally reachable by a network with fully independent nodes. On the other hand, a network of identically behaved nodes optimizes robustness: Any subset of nodes may be removed from the network without any loss of function or expressive power, as long as any single node remains. In addition to considering flexibility across space (nodes), these properties may also vary, largely independently, across time. A network is maximally expressive when its nodes' activity patterns vary in meaningful ways from moment to moment, whereas it is maximally robust to signal corruption when its activity is constant over time. Presumably, most natural systems tend to occupy positions between these temporal and spatial extremes. Under different circumstances, it may even prove beneficial for systems to make different tradeoffs between expressiveness and robustness along the temporal and spatial dimensions. We wondered: might the human brain reconfigure itself to be more flexible or more robust according to ongoing demands? In other words, might the brain reconfigure its connections or behaviors under different circumstances to change its positions along these continuums?

Closely related to the above notions of expressiveness versus robustness are measures of how much information is contained in a given signal or pattern and how redundant a signal is (1). Formally, information is defined as the amount of uncertainty about a given variable's outcomes (i.e., entropy), measured in bits, or the optimal number of yes/no questions needed to reduce uncertainty about the variable's outcomes to zero. Highly

Significance

How our brains respond to ongoing experiences depends on what we are doing and thinking about, among other factors. We examined two fundamental aspects of brain activity under different cognitive circumstances: informativeness and compressibility. Informativeness refers to how specific the brain activity we measure at a given moment is to whatever was being done in that particular moment. Compressibility is a measure of how redundant the activity patterns are. We found that when people were engaged in higher-level cognitive tasks, their brain activity was both more informative and more compressible than when they were engaged in lower-level tasks. Our findings suggest that our brains flexibly reconfigure themselves to optimize different aspects of how they function according to ongoing cognitive demands.

Author contributions: L.L.W.O. and J.R.M. designed research; L.L.W.O. and J.R.M. performed research; L.L.W.O. and J.R.M. analyzed data; J.R.M. obtained funding to support the project; and L.L.W.O. and J.R.M. wrote the

The authors declare no competing interest.

This article is a PNAS Direct Submission. M.B. is a guest editor invited by the Editorial Board.

Copyright © 2024 the Author(s). Published by PNAS. This article is distributed under Creative Commons Attribution-NonCommercial-NoDerivatives License 4.0 (CC BY-NC-ND).

¹To whom correspondence may be addressed. Email: jeremy.r.manning@dartmouth.edu.

This article contains supporting information online at https://www.pnas.org/lookup/suppl/doi:10.1073/pnas. 2400082121/-/DCSupplemental.

Published August 23, 2024.

complex systems with many degrees of freedom (i.e., high flexibility and expressiveness) are more information-rich than simpler or more constrained systems. The redundancy of a signal denotes the difference between how expressive the signal could be (i.e., proportional to the number of unique states or symbols used to transmit the signal) and the actual information rate (i.e., the entropy of each individual state or symbol). If a brain network's nodes are fully independent, then the number of bits required to express a single activity pattern is proportional to the number of nodes. The network would also be minimally redundant since the status of every node would be needed to fully express a single brain activity pattern. If a brain network's nodes are fully coupled and identical, then the number of bits required to express a single activity pattern is proportional to the number of unique states or values any individual node can take on. Such a network would be highly redundant since knowing any individual node's state would be sufficient to recover the full-brain activity pattern. Highly redundant systems are also robust since there is little total information loss due to removing any given observation.

We take as a given that brain activity is highly flexible: Our brains can exhibit nearly infinite varieties of activity patterns. This flexibility implies that our brains' activity patterns are highly information rich. However, brain activity patterns are also highly structured. For example, full-brain correlation matrices are stable within (2-4) and across (4-7) individuals. This stability suggests that our brains' activity patterns are at least partially constrained, for example, by anatomical, external, or internal factors. Constraints on brain activity that limit its flexibility decrease expressiveness (i.e., its information rate). However, constraints on brain activity also increase its robustness to noise (e.g., "missing" or corrupted signals may be partially recovered). For example, recent work has shown that full-brain activity patterns may be reliably recovered from only a relatively small number of implanted electrodes (8, 9). This robustness property

suggests that the relevant signals (e.g., underlying factors that have some influence over brain activity patterns) are compressible.

To the extent that brain activity patterns contain rich taskrelevant information, we should be able to use the activity patterns to accurately differentiate between different aspects of a task (e.g., using pattern classifiers; 10). For example, prior work has shown a direct correspondence between classification accuracy and the information content of a signal (11). To the extent that brain activity patterns are compressible, we should be able to generate simplified (e.g., lower dimensional) representations of the data while still preserving the relevant or important aspects of the original signal. In general, information content and compressibility are often related but are also dissociable (Fig. 1). If a given signal (e.g., a representation of brain activity patterns) contains more information about ongoing cognitive processes, then the peak decoding accuracy should be high. In the simulations shown in Fig. 1C, we construct synthetic datasets that have high or low levels of informativeness by varying temporal autocorrelations in the data (Synthetic Data). If a signal is compressible, then a low-dimensional embedding of the signal will be similarly informative as the original signal. In the simulations shown in Fig. 1C, we construct synthetic datasets that have high or low levels of compressibility by varying the covariance structure across features (Synthetic Data). As shown in Fig. 1D, highly informative datasets yield higher decoding accuracies than less informative datasets (i.e., the peaks of the curves in the Top panels of Fig. 1D are higher than the peaks of the curves in the *Bottom* panels). Highly compressible datasets show steeper slopes when we plot decoding accuracy as a function of the number of components used to represent the data (i.e., the slopes of the curves in the Left panels of Fig. 1D are steeper than the slopes of the curves in the Right panels). Whereas characterizing the informativeness and compressibility of synthetic data can be instructive, we are ultimately interested in understanding how

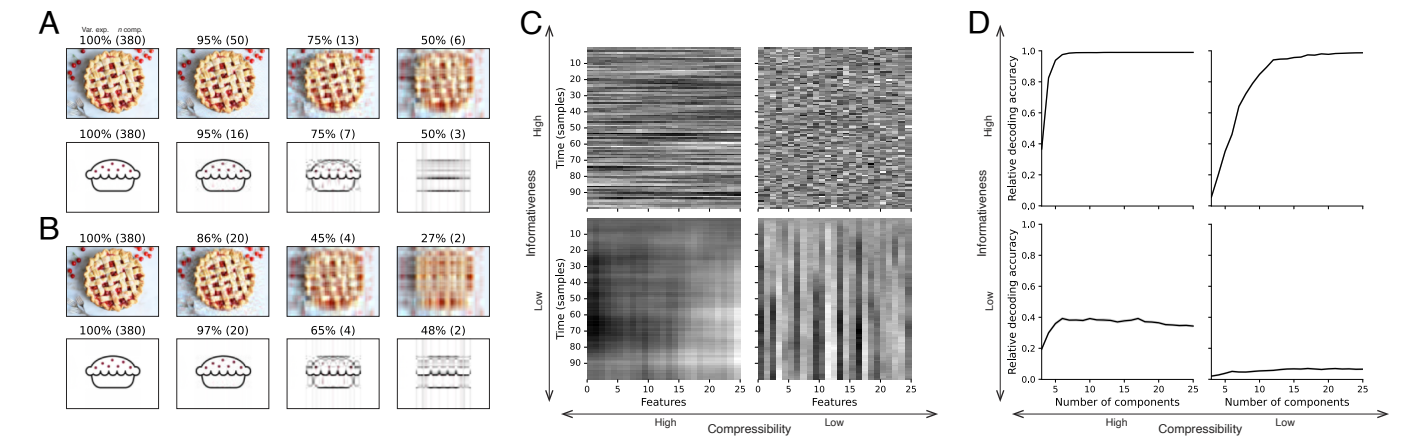


Fig. 1. Information content and compressibility. (A) Variance explained for two images. Consider two example images: a photograph and simple drawing. The images have the same resolutions, but their content is very different. The photograph is more information rich: When we compare the original photograph and drawing (leftmost column), we can see that the photograph captures much more detail. We can also apply principal components analysis to the images, treating the rows of the images as "observations." Across columns, we identified the numbers of components required to explain 100%, 95%, 75%, or 50% of the cumulative variance in each image (the 100% columns denote the original images). The numbers of components are indicated in parentheses, and the resulting "compressed" images are displayed. This analysis reveals that the drawing is more compressible: Just 16 components can explain 95% of the variance in the drawing, whereas 50 components are required to explain 95% of the variance in the photograph. (B) Representing two images with different numbers of components. Using the same principal component decompositions as in Panel (A), we computed the cumulative proportion of variance explained with 380 (original images), 20, 4, or 2 components. This analysis provides another way of characterizing the compressibility of each image by showing that the same number of components can explain more variance in the drawing than in the photograph. (C) Template data from four synthetic datasets. We constructed four synthetic datasets, each comprising 25 features (columns) observed across 100 samples (rows) from each of 10 simulated "participants." The datasets were constructed to contain different levels of informativeness and compressibility (Synthetic Data). (D) Decoding accuracy by number of components. For each synthetic dataset, we trained across-participant classifiers to decode timepoint labels. Each panel displays the decoding accuracy as a function of the number of components used to represent the data. Error ribbons denote bootstrap-estimated 95% CIs.

these properties relate to brain activity patterns recorded under different cognitive circumstances.

Several recent studies suggest that the complexity of brain activity is task-dependent, whereby simpler tasks with lower cognitive demands are reflected by simpler and more compressible brain activity patterns, and more complex tasks with higher cognitive demands are reflected by more complex and less compressible brain activity patterns (12, 13). These patterns hold even when the stimulus itself is held constant (12). These findings complement other work suggesting that functional connectivity (correlation) patterns are task-dependent (3, 7, 8), although see ref. 4. Higher-order cognitive processing of a common stimulus also appears to drive more stereotyped task-related activity and functional connectivity across individuals (14–17).

The above studies are consistent with two potential descriptions of how cognitive processes are reflected in brain activity patterns. One possibility is that the information rate of brain activity increases during more complex or higher-level cognitive processing. If so, then the ability to reliably decode cognitive states from brain activity patterns should improve with task complexity or with the level (or "depth") of cognitive processing. A second possibility is that the compressibility of brain activity patterns decreases during more complex or higher-level cognitive processing. If so, then individual features of brain recordings should carry more information (over and above the information carried by other features) during complex or high-level (versus simple or low-level) cognitive tasks. The tradeoffs between these two aspects of brain activity may also vary across brain regions or networks, for example, according to each region's functional role.

We used a previously collected neuroimaging dataset to estimate the extent to which each of these two possibilities might hold. The dataset we examined comprised functional magnetic resonance imaging (fMRI) data collected as participants listened to an audio recording of a 7-min story, temporally scrambled recordings of the story, or underwent a resting state scan (17). Each of these experimental conditions evokes different depths of cognitive processing (13-15, 17). We used across-participant classifiers to decode listening times in each condition, as a proxy for how "informative" the task-specific activity patterns were (16). We also used principle components analysis to generate lower-dimensional representations of the activity patterns. We then repeated the classification analyses after preserving different numbers of components and examined how classification accuracy changed across the different experimental conditions.

Results

We sought to understand whether higher-level cognition is reflected by more reliable and informative brain activity patterns and how compressibility of brain activity patterns relates to cognitive complexity. We developed a computational framework for systematically assessing the informativeness and compressibility of brain activity patterns recorded under different cognitive circumstances. We used across-participant decoding accuracy (Forward Inference and Decoding Accuracy) as a proxy for informativeness. To estimate the compressibility of the brain patterns, we used group principal components analysis (PCA) to project the brain patterns into k-dimensional spaces, for different values of k [Hierarchical Topographic Factor Analysis (HTFA) and PCA]. For more compressible brain patterns, decoding accuracy should be more robust to small values of k.

We analyzed a dataset collected by Simony et al. (17) that comprised four experimental conditions. These conditions exposed participants to stimuli that systematically varied in cognitive engagement. In the intact experimental condition, participants listened to an audio recording of a 7-min Moth Radio Hour story, Pie Man, by Jim O'Grady. In the paragraph-scrambled experimental condition, participants listened to a temporally scrambled version of the story, where the paragraphs occurred out of order, but where the same set of paragraphs was presented over the entire listening interval. All participants in this condition experienced the scrambled paragraphs in the same order. In the word-scrambled experimental condition, participants listened to a temporally scrambled version of the story, where the words occurred in a random order. Again, all participants in this condition experienced the scrambled words in the same order. Finally, in the rest experimental condition, participants lay in the scanner with no overt stimulus, while keeping their eyes open and blinking as needed. This public dataset provided a convenient means for testing our hypothesis that different levels of cognitive processing and engagement affect how informative and compressible the associated brain patterns are.

To evaluate the relation between informativeness and compressibility for brain activity from each experimental condition, we trained a series of across-participant temporal decoders on compressed representations of the data. Fig. 2A displays the decoding accuracy as a function of the number of principal components used to represent the data (SI Appendix, Figs. S1 and S2). Several patterns were revealed by the analysis. First, in general (i.e., across experimental conditions), decoding accuracy tends to improve as the number of components are increased. However, decoding accuracy peaked at higher levels for experimental conditions that exposed participants to cognitively richer stimuli (Fig. 2D). The peak decoding accuracy was highest for the "intact" condition (versus paragraph: t(99) = 35.205, P < 0.001; versus word: t(99) = 43.172, P < 0.001; versus rest: t(99) = 81.361, P < 0.001), next highest for the "paragraph" condition (versus word: t(99) = 6.243, P < 0.001; versus rest: t(99) = 50.748, P < 0.001), and next highest for the "word" condition (versus rest: t(99) = 48.791, P < 0.001). This ordering implies that cognitively richer conditions evoke more stable brain activity patterns across people.

The cognitively richer conditions also displayed steeper initial slopes. For example, the intact condition decoders reached an arbitrarily chosen threshold of 5% accuracy using fewer components than the paragraph condition decoders (t(99) = -7.429, P < 0.001) or word condition decoders (t(99)) =-7.300, P < 0.001), and decoding accuracy never exceeded 5% for the rest condition. This suggests that brain activity patterns evoked by cognitively richer conditions are more compressible, such that representing the data using the same number of principal components provides more information to the temporal decoders (Fig. 2 B and C). Taken together, as shown in Fig. 2E, we found that brain activity patterns evoked by cognitively richer conditions tended to be both more informative (i.e., associated with higher peak decoding accuracies) and more compressible (i.e., requiring fewer components to achieve the 5% accuracy threshold).

If informativeness (to the temporal decoders) and compressibility vary with the cognitive richness of the stimulus, might these measures also vary over time within a given condition? For example, participants in the intact condition might process the ongoing story more deeply later on in the story (compared with earlier in the story) given the additional narrative background

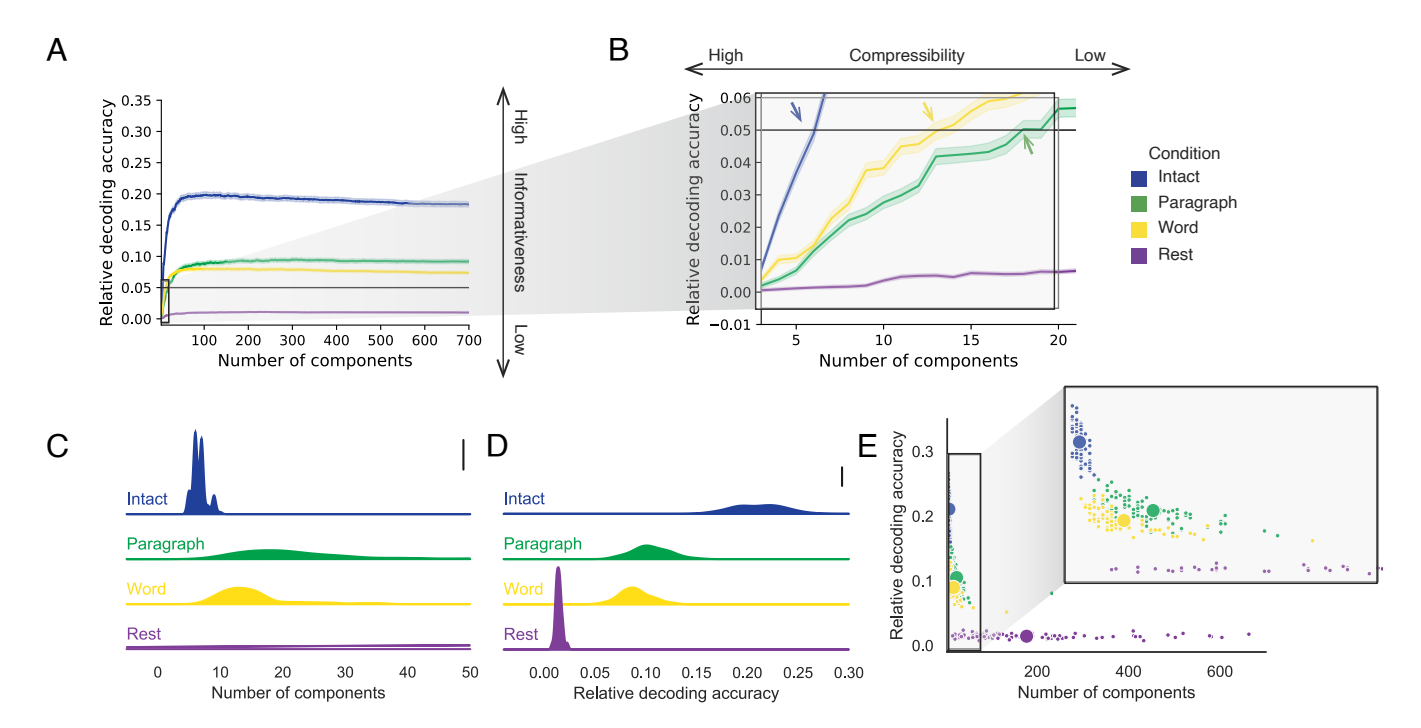


Fig. 2. Decoding accuracy and compression. (A) Decoding accuracy by number of components. Ribbons of each color display cross-validated decoding performance for each condition (intact, paragraph, word, and rest), as a function of the number of components (features) used to represent the data. For each condition, decoding accuracy has been normalized by subtracting expected "chance" decoding performance (estimated as $\frac{1}{T}$, where T is the number of timepoints in the given condition). This normalization was intended to enable fairer comparisons across conditions; a relative decoding accuracy of 0.0 denotes "chance" performance. The horizontal black line denotes 5% decoding accuracy (used as a reference in Panel B). (B) Numbers of components required to reach a fixed decoding accuracy threshold, by condition. The panel displays a zoomed-in view of the Inset in Panel (A). Intersections between each condition's decoding accuracy curve and the 5% decoding accuracy reference line are marked by arrows. All error ribbons in Panels (A and B) denote bootstrap-estimated 95% Cls. (C) Estimating "compressibility" for each condition. The probability density plots display the numbers of components required to reach at least 5% (corrected) decoding accuracy, across all cross-validation runs. For the "rest" condition, where decoding accuracy never reached 5% accuracy, we display the distribution of the numbers of components required to achieve the peak decoding accuracy in each fold. (This distribution is nearly flat, as also illustrated in Panel E). The scale bar denotes a height of 0.01. (D) Estimating "informativeness" for each condition. The probability density plots display the peak (corrected) decoding accuracies achieved in each condition, across all cross-validation runs. The scale bar denotes a height of 0.01. (E) Informativeness versus compressibility. Each dot displays the minimum number of components required to achieve at least 5% corrected decoding accuracy (x-coordinate; for the rest condition, the numbers of components are estimated using the peak decoding accuracies as in Panel C) and the peak (corrected) decoding accuracy (y-coordinate). The smaller dots correspond to individual cross-validation runs and the larger dots display the averages across runs. The Inset displays a zoomed-in view of the indicated region in the main panel.

and context they had been exposed to by that point. To examine this possibility, we divided each condition into four successive time segments. We computed decoding curves (Fig. 3A) and the numbers of components required to achieve 5% decoding accuracy (Fig. 3B) for each segment and condition. We found that, in the two most cognitively rich conditions (intact and paragraph), both decoding accuracy and compressibility, as reflected by the change in decoding curves, increased with listening time (e.g., at the annotated reference point of k = 20components in Fig. 3C: Intact: t(99) = 7.915, P < 0.001; paragraph: t(99) = 2.354, P = 0.021). These changes may reflect an increase in comprehension or depth of processing with listening time. In contrast, the decoding accuracy and compressibility decreased with listening time in the word condition (t(99) = -10.747, P < 0.001) and rest condition (t(99) = -22.081, P < 0.001). This might reflect the depletion of attentional resources in the less-engaging word and rest conditions.

These results make some intuitive sense. As the contextual information available to participants increases (i.e., over time in the cognitively rich intact and paragraph conditions), it makes sense that this might constrain neural responses to a greater extent. While this pattern may not necessarily hold for every possible story or stimulus, we suspect that it is generally the case that our knowledge about what is happening in a story tends to increase as we experience more of it. In turn, this could lead to greater consistency in different people's interpretations of and neural responses to the stimulus. Similarly, as participants are left to "mind wander," or as they experience mental fatigue (i.e., over time in the less cognitively rich word and rest conditions), we suggest that this might lead to greater variability in neural responses across people, resulting in lower decoding accuracy. Again, it is not necessarily the case that every possible "unengaging" stimulus will lead to greater neural variability as time progresses, but we suspect this phenomenon is likely to hold for a variety of such stimuli. These findings replicate at least to a limited extent (e.g., across both cognitively rich conditions and across both cognitively impoverished conditions, and for the different groups of participants in each of those conditions). However, determining whether these patterns generalize to other stimuli (e.g., other scramblings, other stories, other modalities, etc.) would require additional study (with new stimuli).

If the informativeness and compressibility of brain activity patterns vary over time, might these properties also vary across brain networks? We used a network parcellation identified by Yeo et al. (5) to segment the brain into seven distinct networks. The networks can be sorted (roughly) in order from lower-level to higher-level cortex as follows (Fig. 4 A–C): visual, somatomotor,

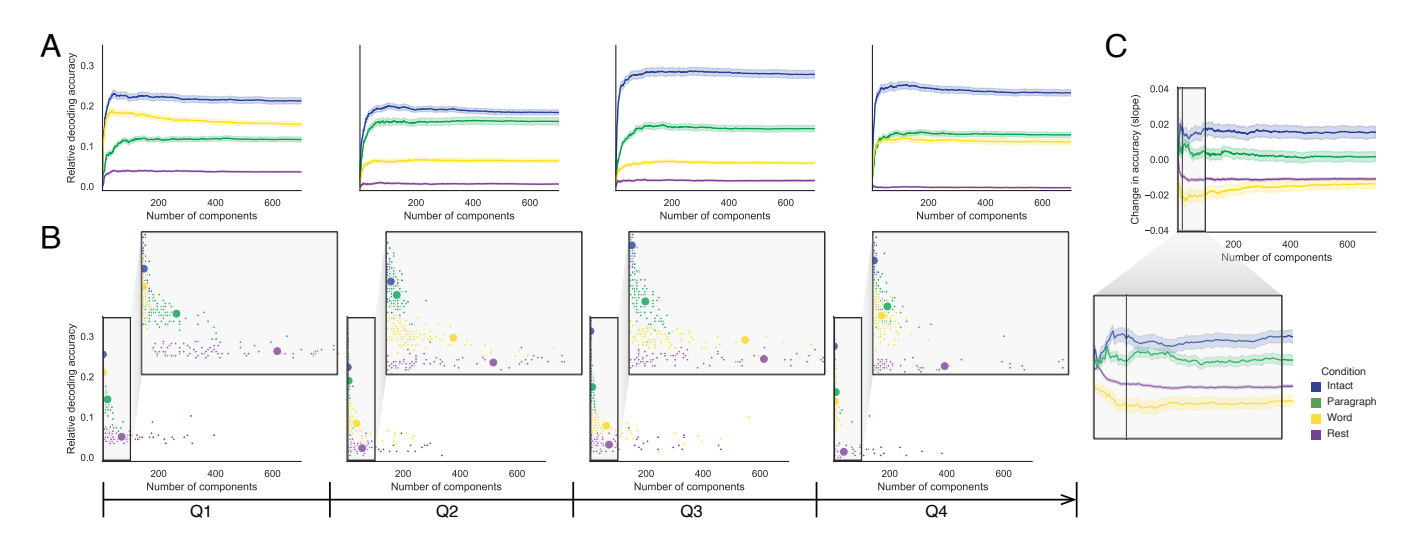


Fig. 3. Changes in decoding accuracy and compression over time. (*A*) Decoding accuracy by number of components, by story segment. Each family of curves is plotted in the same format as Fig. 2*A* but reflects data only from one quarter of the dataset. (*B*) Informativeness versus compressibility by condition and segment. Each scatter plot is in the same format as Fig. 2*E*, but reflects data only from one quarter of the dataset. (*C*) Change in decoding accuracy over time, by number of components. For each number of components (*x*-axis) and condition (color), we fit a regression line to the decoding accuracies obtained for the first, second, third, and fourth quarters of the dataset (corresponding to the columns of Panels *A* and *B*). The *y*-axis denotes the slopes of the regression lines. The black vertical line marks k = 20 components, as referenced in the main text. All error ribbons denote bootstrap-estimated 95% Cls.

dorsal attention, ventral attention, limbic, frontoparietal, and default mode. Next, we computed decoding curves separately for the activity patterns within each network and identified each network's inflection point, for each experimental condition. Moving from low-order networks to higher-order networks, we found that decoding accuracy tended to increase in the higher-level experimental conditions and decrease (slightly) in the lower-level experimental conditions (Fig. 4 D and E; Spearman's rank correlation between decoding accuracy and network order: intact: $\rho = 0.362, P < 0.001;$ paragraph: $\rho = 0.441, P < 0.001;$ word: $\rho = -0.102, P = 0.007;$ rest: $\rho = -0.354$, P < 0.001). This suggests that higher-order networks may carry more content-relevant or stimulus-driven "information." We found no clear trends in the proportions of components required to achieve 5% decoding accuracy across networks or conditions (Fig. 4F). We note that the limbic network we considered here often overlaps with low (imaging) signal regions, and therefore it may be difficult to draw strong conclusions about this network's informativeness or compressibility. We also considered the possibility that the correlations with network order might be influenced by the numbers of nodes in each network. We designed a permutation-based procedure to address this possibility, whereby we repeated the above analyses using shuffled network labels (Network Permutation Tests). The correlations between decoding accuracy and network order were reliably more positive than the shuffled correlations for the intact (t(1,998) = 276.431, P < 0.001) and paragraph (t(1,998) = 330.334, P < 0.001) conditions, and reliably more negative for the word (t(1.998) = -16.386, P < 0.001) and rest (t(1,998) = -318.631, P < 0.001) conditions. These results suggest that the correlations between decoding accuracy and network order were not driven solely by the numbers of nodes in each network.

Whereas the above analyses examined different networks in isolation, how do full-brain (i.e., potentially multinetwork) activity patterns reflected by different principal components vary across different experimental conditions? As shown in Fig. 5, we used Neurosynth (18) to identify, for each component, the associations with each of 80 themes (*Reverse Inference*). In general,

the first principal components across all of the experimental conditions tended to weigh most heavily on themes related to cognitive control, memory, language processing, attention, and perception. Other components appeared to vary more across conditions.

To gain further insights into which brain functions might be most closely associated with the top-weighted components from each experimental condition, we manually grouped each Neurosynth-derived topic into a smaller set of core cognitive functions. Separately for each component, we computed the average weightings across all topics that were tagged as being associated with each of these cognitive functions (Fig. 6A and SI Appendix, Fig. S6 A). To help visualize these associations, we used the patterns of associations for each component to construct graphs whose nodes were experimental conditions and cognitive functions (Fig. 6B and SI Appendix, Fig. S6 B). We also computed correlations between the sets of per-topic weightings from each of the top-weighted components from each experimental condition (Fig. 6 C and D) and between the brain maps for each condition's components (SI Appendix, Fig. S6 *C* and *D*). Taken together, we found that each component appeared to weigh on a fundamental set of cognitive functions that varied by experimental condition. For example, the top principal components from every condition weighed similarly (across conditions) on the full set of Neurosynth topics (Fig. 5A) and cognitive functions (Fig. 6 A and B and SI Appendix, Fig. S6 A and B), suggesting that these components might reflect a set of functions or activity patterns that are common across all conditions. The second components' weightings were similar across the intact, paragraph, and rest conditions (highestweighted functions: cognitive control, memory, social cognition, and resting state), but different for the word condition (highestweighted functions: sensory perception and cognitive control). The fourth components' weighting grouped the paragraph and word conditions (highest-weighted functions: memory, language processing, and cognitive control) and the intact and rest conditions (highest-weighted functions: emotion, social cognition). We also used ChatGPT (19) to sort the list of manually tagged cognitive functions from lowest-level to highest-level

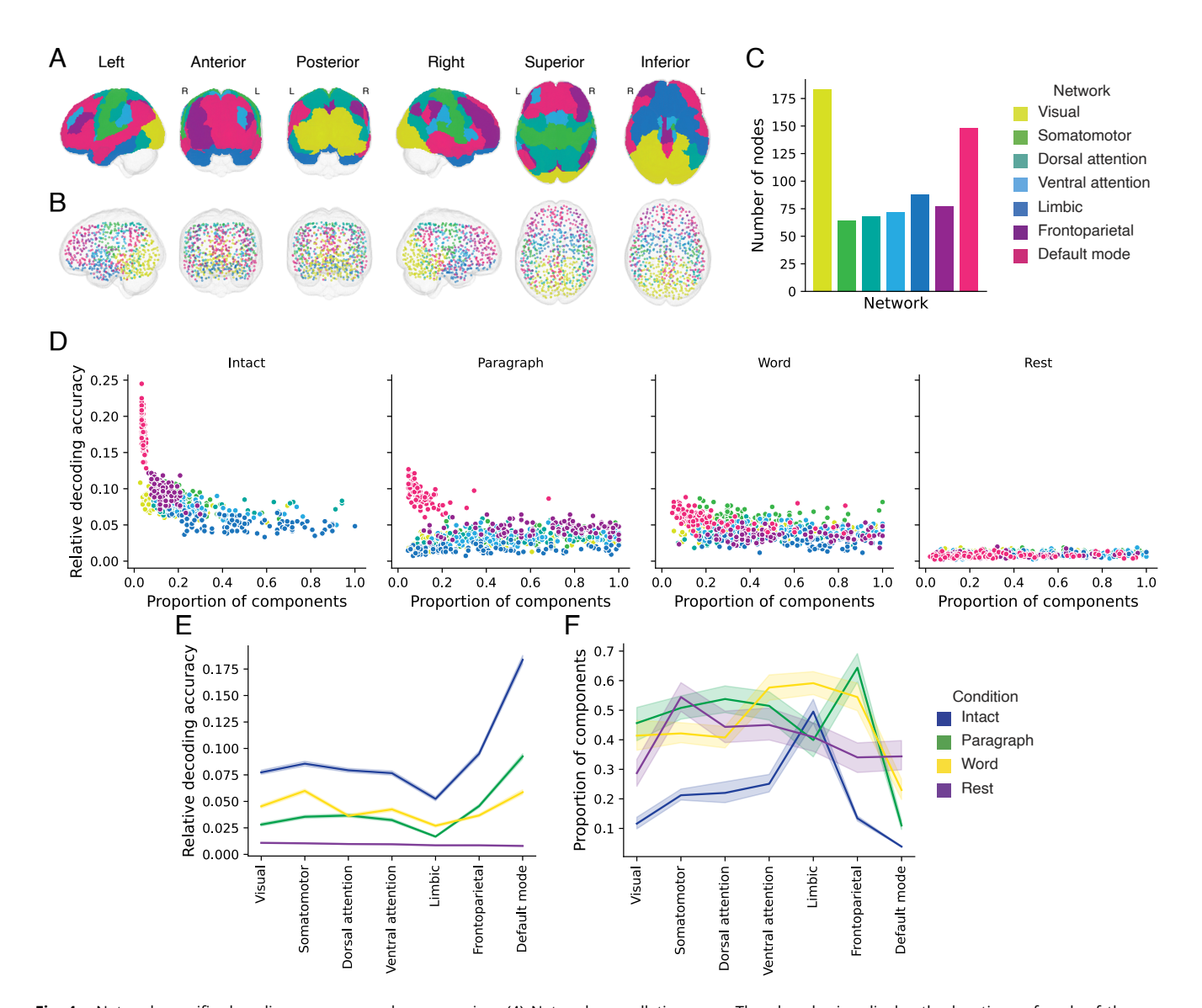


Fig. 4. Network-specific decoding accuracy and compression. (*A*) Network parcellation map. The glass brains display the locations of each of the seven networks identified by Yeo et al. (5). (*B*) Node labels. We assigned network labels to each of the 700 Hierarchical Topographic Factor Analysis-derived nodes [*Hierarchical Topographic Factor Analysis (HTFA)*]. For each node, we evaluated its radial basis function (RBF) at the locations of every voxel in the parcellation map displayed in Panel (*A*). We summed up these RBF weights separately for the voxels in each network. We defined each node's network label as its highest-weighted network across all voxels. The RBF center location of each node is shown as a circle in the glass brains, and the colors denote each node's assigned network label. (*C*) Per-network node counts. The bar plot displays the total number of HTFA-derived nodes assigned to each network. (*D*) Informativeness versus compressibility by network and condition. Each dot corresponds to a single cross-validation run. The dots' coordinates denote the minimum proportion of components (relative to the number of nodes in the given network) required to achieve at least 5% corrected decoding accuracy (*x*-coordinate; for the rest condition these proportions are estimated using the peak decoding accuracies) and peak (corrected) decoding accuracy (*y*-coordinate). We repeated the analysis separately for each network (color) and experimental condition (column). (*E*) Informativeness by network. For each network, sorted (roughly) from lower-order networks on the *Left* to higher-order networks on the *Right*, the curves display the peak (corrected) decoding accuracy for each experimental condition (color). (*F*) Compressibility by network. For each network, the curves display the proportion of components (relative to the total possible number of components displayed in Panel *C*) required to achieve at least 5% decoding accuracy (or, for the rest condition, peak decoding accuracy, as described *Above*).

(SI Appendix, Table S2 and Fig. 6E; also see Ranking Cognitive Processes). We found that higher-level functions tended to be weighted more heavily by top components from the intact and paragraph conditions than lower-level functions (intact versus word: t(198) = 11.059, P < 0.001; intact versus rest: t(198) = 3.699, P < 0.001; paragraph versus word: t(198) = 13.504, p < 0.001; paragraph versus rest: t(198) = 4.812, P < 0.001; also see Ranking Cognitive Processes). The top components from the word condition showed the opposite tendency, whereby lower-level functions tended to be weighted more heavily than higher-level functions (word versus rest:

t(198) = -7.315, P < 0.001). The weighting trends for the intact and paragraph conditions were not reliably different (t(198) = -0.479, P = 0.633). The components from the rest condition showed only a small trending difference in the weights associated with high-level versus low-level functions (rest versus 0: t(99) = 1.836, P = 0.081). These findings suggest that when participants were engaged more strongly (in the more engaging intact and paragraph conditions), their dominant neural patterns reflected higher-level cognitive functions. In contrast, when participants were engaged less strongly (in the less engaging word and rest conditions), their dominant neural

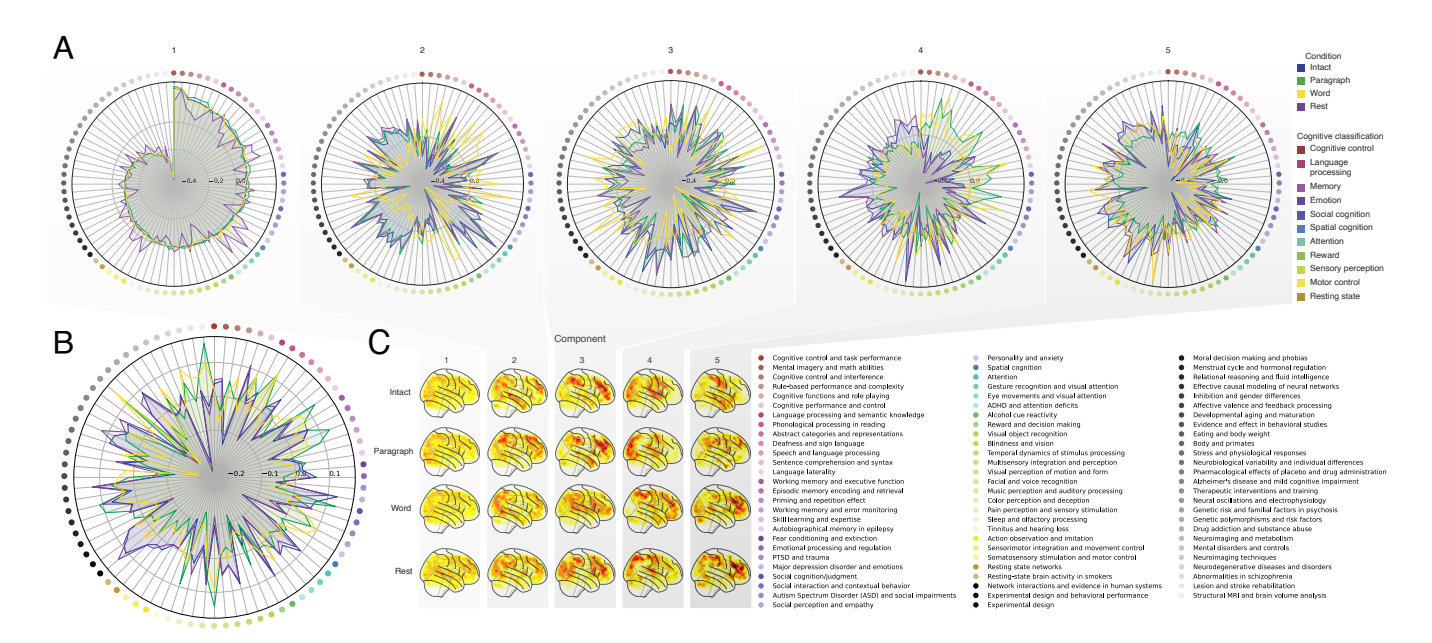


Fig. 5. Neurosynth topic weightings by component. We used a reverse inference procedure (*Reverse Inference*) to estimate the correspondences between brain images and a set of 80 topics derived from the Neurosynth database of neuroimaging articles (18). (A) Topic correlations by component. For each of the top five highest-weighted principal components (columns) derived from each experimental condition (colors), the radar plots display the correlations between the component images and the per-topic images derived for each topic (topic identities are denoted by the colored dots; a legend with high-level labels for each base color is on the *Right*, and a legend with lower-level labels (denoted by tints and shades of each base color) is in the *Lower Right*. An annotated list of the top-weighted topics for each component and condition may be found in *SI Appendix*, Fig. S3 and the *Top*-weighted terms for each topic may be found in *SI Appendix*, Table S1. (B) Topic correlations averaged across components. The radar plot is in the same format as the plots in Panel (A), but here, we display the per-condition average correlations across the top five components (for each condition) reflected in Panel (A). (C) Component images. Each plot displays a right sagittal view of a glass brain projection of the top five principal components (columns) for each experimental condition (rows). Additional projections for each component may be found in *SI Appendix*, Fig. S4.

patterns reflected lower-level cognitive functions. Although they were highly statistically reliable, it is also important to note that these latter effects are also relatively small (e.g., the slopes for all of the experimental conditions are numerically close to zero; Fig. 6*E*). We suggest that this phenomenon may merit further investigation in future work.

Discussion

We examined fMRI data collected as participants listened to an auditory recording of a story, scrambled recordings of the story, or underwent a resting state scan. We found that cognitively richer stimuli evoked more reliable (i.e., consistent across people) and information-rich brain activity patterns. The brain patterns evoked by cognitively richer stimuli were also more compressible, in that each individual component provided more "signal" to temporal decoders relative to components of data from less cognitively rich conditions (Fig. 2). Over time (e.g., as the experiment progressed), these phenomena were strengthened. Specifically, across story segments, data from more cognitively rich conditions became more informative and compressible, and data from less cognitively rich conditions became less informative and compressible (Fig. 3). We also repeated these analyses separately for different brain networks. We found that networks traditionally associated with higher-level cognitive functions tended to provide more informative brain patterns than networks traditionally associated with lower level cognitive functions (Fig. 4). Finally, we examined the most dominant components of the brain activity patterns from each experimental condition. We used a reverse inference approach (18) to identify the terms in the neuroimaging literature most commonly associated with the corresponding maps. As summarized in Fig. 6E, we found that

the intact and paragraph conditions tended to weight higher-level cognitive processes more than lower-level cognitive processes, whereas the word condition weighted lower-level processes more than higher-level processes and the rest condition showed no reliable difference in high-level versus low-level weightings. Taken together, our findings indicate that the informativeness and compressibility of our brain activity patterns are task-dependent and these properties change systematically with factors like cognitive richness and depth of processing.

Our explorations of informativeness and compressibility are related to a much broader literature on the correlational and causal structure of brain activity patterns and networks (5, 13, 20– 38). Correlations or causal associations between different brain regions simultaneously imply that full-brain activity patterns will be compressible and also that those activity patterns will contain redundancies. For example, the extent to which activity patterns at one brain area can be inferred or predicted from activity patterns at other areas (e.g., refs. 8 and 9) reflects overlap in the information available in or represented by those brain areas. If brain patterns in one area are recoverable using brain patterns in another area, then a "signal" used to convey the activity patterns could be compressed by removing the recoverable activity. Predictable (and therefore redundant) brain activity patterns are also more robust to signal corruption. For example, even if the activity patterns at one region are unreadable or unreliable at a given moment, that unreliability could be compensated for by other regions' activity patterns that were predictive of the unreliable region. Whereas compressible brain patterns are robust to spatial signal corruption, high versus low informativeness reflects a similar (though dissociable; e.g., Fig. 1) tradeoff between expressiveness and robustness of temporal patterns. Highly informative brain patterns (by our measure;

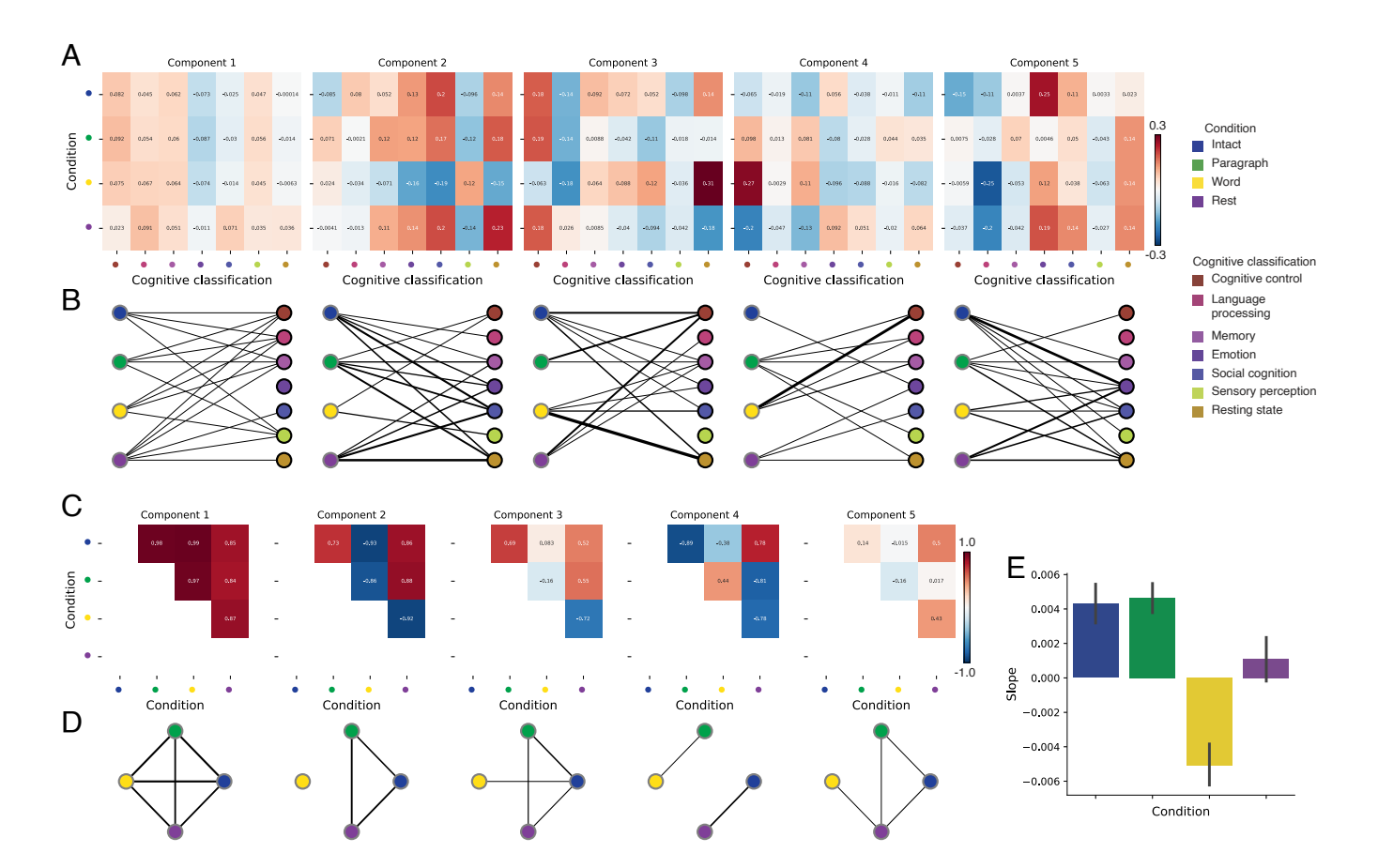


Fig. 6. Summary of functions associated with top-weighted components by condition. (A) Top-weighted topics by condition. Here, we display per-condition (rows, indicated by colored dots) topic correlations, averaged across topics that pertain to each of several broad cognitive functions (columns within each subpanel, indicated by colored dots). Each subpanel reflects correlations for the components indicated in the panel titles. SI Appendix, Table S1 provides a list of each topic's top-weighted terms, along with each topic's manually labeled cognitive classification. A full list of the topics most highly associated with each component may be found in SI Appendix, Fig. S3. (B) Associations between per-condition components and cognitive functions. The network plots denote positive average correlations between the component images for each condition (gray-outlined dots on the Left sides of each network; colors denote conditions) and topic-specific brain maps associated with each indicated cognitive function (black-outlined dots on the Right sides of each network; colors denote cognitive functions). The line thicknesses are proportional to the correlation values (correlation coefficients are noted in the heat maps in Panel A). (C) Correlations between each principal component, by condition. The heat maps display the correlations between the brain maps (SI Appendix, Fig. S4) for each principal component (subpanel), across each pair of conditions (rows and columns of each subpanel's matrix, indicated by colored dots). (D) Associations between per-condition components, by component. Each subpanel's network plot summarizes the pattern of correlations between the nth top-weighted principal components (subpanel) for each experimental condition (gray-outlined dots). The line thicknesses are proportional to the correlation values (correlation coefficients are noted in the heat maps in Panel C). (E) Change in weights by condition. The bar heights reflect the slopes of regression lines, fit separately to the top five components from each condition, between the ChatGPT-derived "rank" of each cognitive classification and the correlations between the component and topic maps associated with cognitive processes at the given rank (Ranking Cognitive Processes) Error bars denote bootstrap-estimated 95% Cls. Also see SI Appendix, Fig. S6 for additional information.

i.e., patterns that yield greater temporal decoding accuracy) are expressive about ongoing experiences or cognitive states, since each moment's pattern is reliably distinguishable from other moments' patterns. However, when each moment's pattern is unique, brain activity becomes less robust to temporal signal corruption. Our finding that brain activity patterns becomes more informative (i.e., less robust to temporal signal corruption) and compressible (i.e., more robust to spatial signal corruption) when cognitive engagement is higher suggests that our brain may optimize its activity patterns to prioritize either temporal or spatial robustness, according to task demands.

Our findings that informativeness and compressibility change with task demands may follow from task-dependent changes in full-brain correlation patterns. A number of prior studies have found that so-called "functional connectivity" (i.e., correlational) patterns vary reliably across tasks, events, and situations (7, 13, 17, 39). By examining how these task-dependent changes in correlations affect informativeness and compressibility, our work suggests a potential reason why the statistical structure of brain activity patterns might vary with cognitive task or with cognitive demands. For lower-level tasks, or for tasks that require relatively little "deep" cognitive processing, our brains may optimize activity patterns for robustness and redundancy over expressiveness, for example, to maximize reliability. For higher-level tasks, or for tasks that require deeper cognitive processing, our brains may sacrifice some redundancy in favor of greater expressiveness.

One potential limitation of our work concerns how our measure of informativeness might generalize across different tasks, cognitive representations, and processes. As in many neuroimaging studies, our findings may also be influenced by our preprocessing decisions, which could in turn affect temporal and spatial correlations in the data. Our use of across-participant temporal decoding accuracy as a proxy for informativeness is motivated in part by prior work that introduced acrossparticipant similarity (in time-varying response to a stimulus) as a

means of identifying stimulus-driven brain activity patterns (17). Intuitively, only activity patterns that are driven by the stimulus would be expected to synchronize (i.e., be time-locked to the stimulus) across participants. This approach implicitly removes idiosyncratic responses (e.g., neural patterns that are not similar across people). However, there are also some published examples, including in our own prior work, that indicate that some types of stimulus-evoked activity will be missed by across-participant comparisons. For example we have reported how brain regions like the ventromedial prefrontal cortex (vmPFC) show stimulusdriven responses that are, for the most part, not similar across people (40). In that paper (and drawing on other work), we suggest that the vmPFC seems to represent or support highly idiosyncratic internal states, like affective responses. Although we would consider the vmPFC to be a "high-level" region (e.g., we consider affect to be a relatively high-level aspect of cognition), the measure of informativeness that we used in our current study would identify regions like the vmPFC as having low informativeness. This is because across-participant decoding accuracy (our proxy measure for informativeness) will only be high for representations or responses that are common across people.

Relatedly, even in the experimental conditions we describe as "less cognitively engaging," we think it likely that highlevel thought or cognitive processing is still present. Rather, we suggest that these high-level representations will tend to be more idiosyncratic when the stimulus is less engaging, and therefore less constraining on people's thoughts. Nonetheless, even during highly engaging tasks, people may engage in idiosyncratic stimulus-driven processes. For example, people might retrieve personal information as they listened to the story. Those retrievals could happen at different times for different people according to each individual's prior experiences. Even when those sorts of retrievals happen to be temporally synchronized across people, the specific memories or information being retrieved might still be idiosyncratic. Our measure of informativeness is insensitive to these processes. Further, even in response to an identical stimulus, task instructions or participants' internal goals could change the relationship between compressibility and informativeness. Some work has shown that the "dimensionality" of neural representations can change systematically with task complexity, even in response to an identical stimulus (12). Taken together, we expect that the way we have defined informativeness in this paper, and the specific dataset we examined, are likely to have influenced our findings. While we see our approach as a reasonable first step, we also suggest that future work should explore alternative measures of informativeness and compressibility, and should examine how these measures vary across different tasks and

In the information theory sense (1), when a signal is transmitted using a fixed alphabet of "symbols," the information rate decreases as the signal is compressed (e.g., fewer symbols transmitted per unit time, using an alphabet with fewer symbols, etc.). Our finding that each individual brain component (symbol) become more informative as cognitive richness increases suggests that the "alphabet" of brain activity patterns is also task-dependent. Other work suggests that the representations that are reflected by brain activity patterns may also change with task demands. For example, our brains may represent the same perceptual stimulus differently depending on which aspects of the stimulus or which combinations of features are task-relevant (12).

We found that different brain networks varied in how informative and compressible their activity patterns were across experimental conditions (e.g., Fig. 4). This might follow from evolutionary optimizations that reflect the relevant constraints

or demands placed on those networks. One possibility is that the cortex is organized in a hierarchy of networks "concerned with" or selective to different levels of processing or function. To the extent that different levels of processing (e.g., low-level sensory processing versus "deeper" higher-level processing) reflect different stimulus timescales (e.g., ref. 41), the network differences we observed might also relate to the timescales at which each network is maximally sensitive (14, 15, 42, 43).

Our reverse inference analyses (Figs. 5 and 6) also provide some insights into how neural activity patterns change with cognitive engagement or task demands. Prior work has shown that the components and network "parcels" identified through covarying activity patterns can be highly similar even across different tasks (including "rest," e.g., refs. 39 and 44). We replicated this basic finding in that the first principal components from all four experimental conditions were strikingly similar (e.g., see the leftmost columns of Figs. 5A and 6 C and D). We also found some small, though statistically reliable, systematic changes in the weights associated with different cognitive functions across conditions (Fig. 6E). This result provided an additional way of characterizing network-level differences across conditions (Fig. 4E). Taken together, these findings suggest that although similar networks may be involved in different tasks, the ways in which those networks are engaged may vary systematically with task demands.

Concluding Remarks. Cognitive neuroscientists are still grappling with basic questions about the fundamental "rules" describing how our brains respond, and about how brain activity patterns and the associated underlying cognitive representations and computations are linked. We identified two aspects of brain activity patterns, informativeness and compressibility, that appear to change systematically with task demands and across brain networks. We speculate that these changes may reflect ongoing tradeoffs between how robust to signal corruption versus how expressive about ongoing cognitive states our brains' activity patterns are. Our work also provides a framework for evaluating these tradeoffs in other datasets, or in future studies.

Materials and Methods

We measured properties of recorded neuroimaging data under different task conditions that varied systematically in cognitive engagement and depth of processing. We were especially interested in how informative and compressible the activity patterns were under these different conditions (Fig. 1).

Unless otherwise noted, all statistical tests are two-sided, all error bars and error ribbons denote bootstrap-estimated 95% CIs across participants, and all reported *P*-values are corrected for multiple comparisons using the Benjamini-Hochberg procedure (45).

Functional Neuroimaging Data Collected during Story Listening. We examined an fMRI dataset collected by Simony et al. (17) that the authors have made publicly available at arks.princeton.edu/ark:/88435/dsp015d86p269k. The dataset comprises neuroimaging data collected as participants listened to an audio recording of a story (intact condition; 36 participants), listened to temporally scrambled recordings of the same story (17 participants in the paragraph-scrambled condition listened to the paragraphs in a randomized order and 36 in the word-scrambled condition listened to the words in a randomized order), or lay resting with their eyes open in the scanner (rest condition; 36 participants). Full neuroimaging details may be found in the original paper for which the data were collected (17). Procedures were approved by the Princeton University Committee on Activities Involving Human Subjects, and by the Western Institutional Review Board. All subjects were native English speakers with normal hearing and provided written informed consent. We have

excerpted the relevant portions of the dataset documentation here to provide information about the scanning parameters and preprocessing steps used to generate the data we analyzed (the original descriptions may be found at the above link):

Subjects were scanned in a 3T full-body MRI scanner (Skyra; Siemens) with a 16-channel head coil. For functional scans, images were acquired using a T2* weighted echo planer imaging pulse sequence [repetition time (TR), 1,500 ms; echo time (TE), 28 ms; flip angle, 64°], each volume comprising 27 slices of 4 mm thickness with 0 mm gap; slice acquisition order was interleaved. In-plane resolution was $3 \times 3 \,\mathrm{mm}^2$ [field of view (FOV), $192 \times 192 \,\mathrm{mm}^2$]. Anatomical images were acquired using a T1-weighted magnetization-prepared rapidacquisition gradient echo pulse sequence (TR, 2,300 ms; TE, 3.08 ms; flip angle 9° ; 0.89 mm³ resolution; FOV, 256 mm²). To minimize head movement, subjects' heads were stabilized with foam padding. Stimuli were presented using the Psychophysics toolbox (46, 47). Subjects were provided with an MRI-compatible in-ear monoearbuds (Sensimetrics Model S14), which provided the same audio input to each ear. MRI-safe passive noise-canceling headphones were placed over the earbuds, for noise removal and safety.

Functional data were preprocessed and analyzed using FSL (Functional Magnetic Resonance Imaging of the Brain Software Library; www.fmrib.ox.ac.uk/fsl), including correction for head motion and slice-acquisition time, spatial smoothing (6 mm full width half maximum Gaussian kernel), and high-pass temporal filtering (140 s period). Preprocessed data were aligned to coplanar and high-resolution anatomicals and the standard MNI152 brain, and interpolated to 3-mm isotropic voxels.

The intact and word conditions each comprised 300 TRs (7.5 min) per participant. The paragraph condition comprised 272 TRs (6.8 min) per participant. The rest condition comprised 400 TRs (10 min) per participant.

HTFA. Following our prior related work, we used HTFA (48) to derive a compact representation of the neuroimaging data. In brief, this approach approximates the timeseries of voxel activations (44,415 voxels) using a much smaller number of radial basis function (RBF) nodes (in this case, 700 nodes, as determined by an optimization procedure; 48). This provides a convenient representation for examining full-brain activity patterns and network dynamics. All of the analyses we carried out on the neuroimaging dataset were performed in this lowerdimensional space. In other words, each participant's data matrix was a number of timepoints (7) by 700 matrix of HTFA-derived factor weights (where the row and column labels were matched across participants). Code for carrying out HTFA on fMRI data may be found as part of the BrainIAK toolbox (49), which may be downloaded at brainiak.org.

We also considered alternative approaches to obtaining compact representations of the neuroimaging data, including network parcellations (e.g., refs. 50 and 51). Whereas network parcellations are typically derived from large resting state datasets, HTFA may be applied to much smaller datasets. In our prior work, we showed that HTFA applied to the same dataset used here can explain full-brain activity to within a maximum of 0.25 SDs of each voxel's observed activity in the original dataset, taken across all voxels, images, and participants, using the 700-node representation we also employed here (48). Some of the explanatory power of HTFA comes from the fact that each node's influence falls off smoothly with distance to its center. Intuitively, the result is a representation that looks like a lightly spatially smoothed version of the original data, but where the degree of smoothing varies across the brain according to how spatially autocorrelated the local activity patterns are.

Network Permutation Tests. In our analyses of how informativeness varied across brain networks (Fig. 4), we considered the possibility that the correlations with network order might be influenced by the numbers of nodes in each network. We designed a permutation-based procedure to address this possibility, whereby we repeated the above analyses using shuffled network labels. Specifically, for each of $n_1 = 10$ iterations, we randomly shuffled (without replacement) the network labels of the HTFA nodes, and then we reran our entire decoding analysis pipeline, including applying PCA with 3...m features for each condition (where m is the number of nodes in the given network), and then running 100 cross-validation runs of the decoding procedure for each condition and number of components. This resulted in 10 sets of shuffled data, where each network had the same numbers of nodes, but where the decoding results no longer maintained the fidelity of each individual network. Note that, for each of the shuffled datasets, the same shuffled labels were used for all participants.

We sampled the original and shuffled datasets (with replacement) to create $n_2 = 1,000$ bootstrap samples. For each bootstrap sample, we computed the correlations between the decoding accuracies and network order for each condition and number of components. This yielded a distribution of n_2 correlation values for each condition, for both the original and shuffled datasets. We then compared the distributions of Spearman's ρ values for the original and shuffled datasets using two-sided independent samples Welch's t tests.

PCA. We applied group PCA(52) separately to the HTFA-derived representations of the data (i.e., factor loadings) from each experimental condition. Specifically, for each condition, we considered the set of all participants' T by 700 factor weight matrices. We used group PCA to project these 700-dimensional matrices into a series of shared k-dimensional spaces, for $k \in \{3, 4, 5, ..., 700\}$. This yielded a set of number-of-participants matrices, each with T rows and k columns.

Temporal Decoding. We sought to identify neural patterns that reflected participants' ongoing cognitive processing of incoming stimulus information. As reviewed by Simony et al. (17), one way of homing in on these stimulus-driven neural patterns is to compare activity patterns across individuals. In particular, neural patterns will be similar across individuals to the extent that the neural patterns under consideration are stimulus-driven, and to the extent that the corresponding cognitive representations are reflected in similar spatial patterns across people (16). Following this logic, we used an across-participant temporal decoding test developed by Manning et al. (48) to assess the degree to which different neural patterns reflected ongoing stimulus-driven cognitive processing across people. The approach entails using a subset of the data to train a classifier to decode stimulus timepoints (i.e., moments in the story participants listened to) from neural patterns. We use decoding (forward inference) accuracy on held-out data, from held-out participants, as a proxy for the extent to which the inputted neural patterns reflected stimulus-driven cognitive processing in a similar way across individuals.

Forward inference and decoding accuracy. We used an across-participant correlation-based classifier to decode which stimulus timepoint matched each timepoint's neural pattern. For a given value of k (i.e., number of principal components), we first used group PCA to project the data from each condition into a shared k-dimensional space. Next, we divided the participants into two groups: a template group, $\mathcal{G}_{template}$ (i.e., training data), and a to-be-decoded group, $\mathcal{G}_{\text{decode}}$ (i.e., test data). We averaged the projected data within each group to obtain a single T by k matrix for each group. Next, we correlated the rows of the two averaged matrices to form a T by T decoding matrix, Λ . In this way, the rows of Λ reflected timepoints from the template group, while the columns reflected timepoints from the to-be-decoded group. We used Λ to assign temporal labels to each timepoint (row) from the test group's matrix, using the row of the training group's matrix with which it was most highly correlated. We repeated this decoding procedure, but using \mathcal{G}_{decode} as the template group and $\mathcal{G}_{template}$ as the to-be-decoded group. Given the true timepoint labels (for each group), we defined the decoding accuracy as the average proportion of correctly decoded timepoints, across both groups (where chance performance is $\frac{1}{\tau}$). In Figs. 2 and 3, we report the decoding accuracy for each condition and value of k, averaged across n = 100 cross-validation folds.

Reverse Inference. To help interpret the brain activity patterns we found within the contexts of other studies, we created summary maps of each principal component, for each experimental condition. Each principal component comprises 700 "weights" on each of the HTFA-derived RBF nodes (HTFA). For each node, we evaluated its RBF at the locations of every voxel in the standard

2 mm MNI152 template brain and multiplied the RBF by the node's weight. The sum of these weighted RBF activation maps provides a full-brain image, in MNI152 space, of the given principal component (*SI Appendix*, Fig. S4).

Next, we considered 80 topics estimated using Latent Dirichlet Allocation (53) applied to 9,204 functional neuroimaging articles in the Neurosynth database (18). The topics, as well as associated brain maps identified using Neurosynth, were identified and reported in several prior studies (54-56). The topic labels for each topic were generated automatically with the following ChatGPT (19) prompt: "Please help me come up with intuitive labels for topics I found by fitting a topic model to thousands of neuroscience and psychology articles. I'll paste in the top 10 highest-weighted words for each topic, and I'd like you to respond with a suggested label. For each topic, please respond with just the topic label and no other formatting or text. Here are the next topic's top words": followed by a comma-separated list of the given topic's top-weighted words reflected in SI Appendix, Table S1. For some topics, ChatGPT responded with a longer-form response rather than a concise topic label. In these instances, on a case-by-case basis, we used a second follow-up prompt to achieve the given topic's label: "Could you please come up with a more concise label for that topic?" We then manually identified a set of 11 cognitive labels that were intended to encapsulate a representative range of widely studied low-level and high-level cognitive functions. In choosing the set of cognitive labels, we jointly considered each topic's ChatGPT-derived topic label, along with the top-weighted words for the topic. We attempted to generate a concise set of labels that still spanned the full set of cognitive functions reflected across the 80 topics. Topics that appeared unrelated to specific cognitive functions (e.g., topics related to specific methods or clinical themes) are designated with dashes in SI Appendix, Table S1.

Finally, following an approach used in several prior studies (54–56), we treated the correlation between a given component's brain map and each topic's brain map as an approximate measure of how much the component was reflective of the given topic. This resulted in a set of 80 "weights" (correlation coefficients) for each component's brain map, with one weight per Neurosynth-derived topic.

Ranking Cognitive Processes. We manually identified 11 cognitive labels spanning the set of 80 Neurosynth-derived topics: cognitive control, language processing, memory, emotion, social cognition, spatial cognition, attention, reward, sensory perception, motor control, and resting state. We then used ChatGPT to automatically "rank" the processes from high-level to low-level using the following prompt: "Please rank these cognitive processes from highest-level to lowest-level, where higher values indicate higher-order or higher-level processes. Return the result as a csv file with a header row and two columns: 'Cognitive label' and 'Rank.' Here are the processes: cognitive control, language processing, memory, emotion, social cognition, spatial cognition, attention, reward, sensory perception, motor control, resting state." SI Appendix, Table S2 displays the output.

We recognize that ChatGPT is not omniscient, nor should it be treated as an expert cognitive neuroscientist. We therefore reviewed ChatGPT's responses carefully by hand to verify that they seemed reasonable to us. Whereas prior work has often constructed such rankings by hand, we see our use of ChatGPT in this case as a small additional "sanity check" on our rankings that helped us to be slightly more objective than if we had simply created the rankings ourselves manually.

In the analysis presented in Fig. 6E, we summarize difference in topic weightings across experimental conditions. In particular, we sought to characterize how the dominant neural patterns evoked by each experimental condition weighted on different cognitive functions. For each of the top five principal components from each experimental condition (Fig. 5), we computed the average weights for each of the 11 manually identified (and ChatGPT-ranked) cognitive labels described above (SI Appendix, Table S2). We then fit a line separately for each experiment condition (x-values: cognitive rank; y-values: weights). In carrying out this analysis, we used a bootstrap procedure

- 1. C. E. Shannon, A mathematical theory of communication. Bell Syst. Tech. J. 27, 379-423 (1948).
- E. S. Finn et al., Functional connectome fingerprinting: Identifying individuals using patterns of brain connectivity. Nat. Neurosci. 18, 1664–1671 (2015).
- E. S. Finn et al., Can brain state be manipulated to emphasize individual differences in functional connectivity. Neurolmage 160, 140–151 (2017).
- C. Gratton et al., Functional brain networks are dominated by stable group and individual factors, not cognitive or daily variation. Neuron 98, 439–452 (2018).

to estimate the variability in the slopes of the regression lines, whereby we repeated this process for each of n=100 iterations, each time resampling (with replacement) the set of observed ranks and weights. This procedure yielded distributions of 100 estimated slopes for each experimental condition. We used these distributions to compare the slopes across experimental conditions and to estimate 95% CIs.

Synthetic Data. To help illustrate the relationship between informativeness and compressibility (Fig. 1), we generated four synthetic datasets, varying in informativeness and compressibility. Each dataset comprised simulated observations of k=25 features across n=100 timepoints, from each of S=10 participants. To create each dataset, we first constructed a "template" matrix of N timepoints by K features. We then generated participant-specific data by adding independent noise to each entry in template matrix, drawn from the unit normal distribution (i.e., with a mean of 0 and a variance of 1). We repeated this process for each participant, yielding S participant-specific matrices for each dataset.

Since we estimate informativeness using the temporal decoding accuracy across participants, highly informative data will tend to have observations that are highly timepoint specific. Relatively uninformative data, in contrast, will tend to have more similar observations across timepoints. To generate data with "high informativeness," we constructed template matrices whose rows (observations) were drawn independently from zero-mean multivariate normal distributions. The covariances of these distributions were determined according to the desired compressibility of the data, as described below. We used a multistep process to generate data with "low informativeness." First, we generated new template matrices using the same procedure as for the "high informativeness" datasets. We then multiplied each matrix by a constant ($\rho=0.1$) and computed the cumulative sum of each matrix's rows. This yielded matrices whose rows were highly similar across observations.

Compressibility reflects the extent to which decoding accuracy is affected by reducing the number of components used to represent the data. Highly compressible data will tend to exhibit more similarities across features, whereas less compressible data will tend to show greater independence across features. To generate data with "high compressibility," we set the covariance matrix of the multivariate normal distribution to a Toeplitz matrix whose first row was given by [K, K-1, ..., 1]. To generate data with "low compressibility," we set the covariance matrix to the identity matrix.

Template matrices for datasets with high informativeness and high compressibility, high informativeness and low compressibility, low informativeness and high compressibility, and low informativeness and low compressibility are displayed in Fig. 1*C*. The corresponding decoding curves are displayed in Fig. 1*D*.

Data, Materials, and Software Availability. All of the code used to produce the figures and results in this manuscript, along with links to the corresponding data, may be found at github.com/ContextLab/pca_paper (57).

ACKNOWLEDGMENTS. We acknowledge discussions with Rick Betzel, Luke Chang, Emily Finn, and Jim Haxby. Ourwork was supported in part by NSF CAREER Award Number 2145172 to J.R.M. The content is solely the responsibility of the authors and does not necessarily represent the official views of our supporting organizations. The funders had no role in study design, data collection and analysis, decision to publish, or preparation of the manuscript.

Author affiliations: ^a Department of Psychiatry and Human Behavior, Carney Institute for Brain Sciences, Brown University, Providence, RI 02906; ^b Department of Psychological and Brain Sciences, Dartmouth College, Hanover, NH 03755; and ^c Department of Computer Science, University of Montana, Missoula, MT 59812

- B. T. T. Yeo et al., The organization of the human cerebral cortex estimated by intrinsic functional connectivity. J. Neurophysiol. 106, 1125–1165 (2011).
- E. Glerean, J. Salmi, J. M. Lahnakoski, I. P. Jääskeläinen, M. Sams, Functional magnetic resonance imaging phase synchronization as a measure of dynamic functional connectivity. *Brain Connect.* 2, 91–101 (2012).
- M. W. Cole, D. S. Bassett, J. D. Power, T. S. Braver, S. E. Petersen, Intrinsic and task-evoked network architectures of the human brain. *Neuron* 83, 238–251 (2014).

- L. L. W. Owen et al., A Gaussian process model of human electrocorticographic data. Cereb. Cortex 30, 5333-5345 (2020).
- K. W. Scangos et al., Biomarkers of depression symptoms defined by direct intracranial neurophysiology. Front. Hum. Neurosci. 15, 746499 (2021).
- K. A. Norman, S. M. Polyn, G. J. Detre, J. V. Haxby, Beyond mind-reading: multi-voxel pattern analysis of fMRI data. Trend. Cogn. Sci. 10, 424-430 (2006).
- S. A. Alvarez, An Exact Analytical Relation Among Recall, Precision, and Classification Accuracy in Information Retrieval (Boston College, 2002).
- M. L. Mack, A. R. Preston, B. C. Love, Ventromedial prefrontal cortex compressesion during concept learning. Nat. Commun. 11, 46 (2020).
- L. L. W. Owen, T. H. Chang, J. R. Manning, High-level cognition during story listening is reflected in high-order dynamic correlations in neural activity patterns. *Nat. Commun.* **12**, 5728 (2021).
- U. Hasson, E. Yang, I. Vallines, D. J. Heeger, N. Rubin, A hierarchy of temporal receptive windows in human cortex. *J. Neurosci.* **28**, 2539–2550 (2008).
- Y. Lerner, C. J. Honey, L. J. Silbert, U. Hasson, Topographic mapping of a hierarchy of temporal receptive windows using a narrated story. *J. Neurosci.* **31**, 2906–2915 (2011).
- E. Simony, C. Chang, Analysis of stimulus-induced brain dynamics during naturalistic paradigms. NeuroImage 216, 116461 (2020).
- E. Simony, C. J. Honey, J. Chen, U. Hasson, Dynamic reconfiguration of the default mode network during narrative comprehension. Nat. Commun. 7, 1-13 (2016).
- T. N. Rubin et al., Decoding brain activity using a large-scale probabilistic functional-anatomical atlas of human cognition. PLoS Comput. Biol. 13, e1005649 (2017).
- OpenAl, ChatGPT (2023). https://chat.openai.com. Accessed 15 March 2023.
- M. G. Preti, T. A. W. Bolton, D. Van De Ville, The dynamic functional connectome: State-of-the-art and perspectives. NeuroImage 160, 41-54 (2017).
- B. P. Rogers, V. L. Morgan, A. T. Newton, J. C. Gore, Assessing functional connectivity in the human brain by fMRI. Magn. Reson. Imaging 25, 1347-1357 (2007).
- M. Rubinov, O. Sporns, Complex network measures of brain connectivity: Uses and interpretations. Neurolmage 52, 1059-1069 (2010).
- 23. A. E. Sizemore et al., Cliques and cavities in the human connectome. J. Comput. Neurosci. 44, 115-145 (2018).
- 24. S. M. Smith et al., Resting-state fMRI in the human connectome project. NeuroImage 80, 144-168 (2013).
- 25. S. M. Smith et al., Functional connectomics from resting-state fMRI. Trend. Cogn. Sci. 17, 666-682 (2013).
- 26. R. Srinivasan, W. R. Winter, J. Ding, P. L. Nunez, EEG and MEG coherence: Measures of functional connectivity at distinct spatial scales of neocortical dynamics. J. Neurosci. Methods 166, 41-52 (2007).
- D. Tomasi, N. D. Volkow, Association between functional connectivity hubs and brain networks. Cereb. Cortex 21, 2003-2013 (2011).
- Y. Adachi et al., Functional connectivity between anatomically unconnected areas is shaped by collective network-level effects in the macaque cortex. Cereb. Cortex 22, 1586-1592
- 29. D. S. Bassett, O. Sporns, Network neuroscience. Nat. Neurosci. 20, 353-364 (2017).
- E. Bullmore, O. Sporns, Complex brain networks: graph theoretical analysis of structural and functional systems. Nat. Rev. Neurosci. 10, 186-198 (2009).
- O. Sporns, C. J. Honey, Small worlds inside big brains. Proc. Natl. Acad. Sci. USA 103, 19219-19220 (2006).
- 32. O. Sporns, R. F. Betzel, Modular brain networks. Annu. Rev. Psychol. 67, 613-640 (2016).

- 33. O. Sporns, J. D. Zwi, The small world of the cerebral cortex. Neuroinformatics 2, 145-162 (2004).
- M. Dhamala, G. Rangarajan, M. Ding, Analyzing information flow in brain networks with nonparametric Granger causality. NeuroImage 41, 354-362 (2008).
- A. Korzeniewska, C. M. Crainiceanu, R. Kus, P. J. Franaszczuk, N. E. Crone, Dynamics of eventrelated causality in brain electrical activity. Hum. Brain Mapp. 29, 1170-1192 (2008).
- A. Brovelli et al., Beta oscillations in a large-scale sensorimotor cortical network: Directional influences revealed by Granger causality. Proc. Natl. Acad. Sci. USA 101, 9849-9854 (2004).
- C. W. Lynn, D. S. Bassett, Quantifying the compressibility of complex networks. Proc. Natl. Acad. Sci. USA 118, e2023473118 (2021).
- M. Shinn et al., Functional brain networks reflect spatial and temporal autocorrelation. Nat. Neurosci. 26, 867-878 (2023).
- S. M. Smith et al., Correspondence of the brain's functional architecture during activation and rest. Proc. Natl. Acad. Sci. USA 106, 13040–13045 (2009).
- L. J. Chang et al., Endogenous variation in ventromedial prefrontal cortex state dynamics during naturalistic viewing reflects affective experience. Sci. Adv. 7, eabf7129 (2021).
- J. R. Manning, Context Reinstatement in Handbook of Human Memory M. J. Kahana, A. D. Wagner, Eds. (Oxford University Press, 2023).
- M. Regev et al., Propagation of information along the cortical hierarchy as a function of attention while reading and listening to stories. Cereb. Cortex 29, 4017-4034 (2018).
- C. Baldassano et al., Discovering event structure in continuous narrative perception and memory. Neuron 95, 709-721 (2017).
- A. R. Laird et al., Behavioral interpretations of intrinsic connectivity networks. J. Cogn. Neurosci. 23, 4022-4037 (2011).
- Y. Benjamini, Y. Hochberg, Controlling the False Discovery Rate: A practical and powerful approach to multiple testing. J. R. Stat. Soc. Ser. B 57, 289-300 (1995).
- D. H. Brainard, The psychophysics toolbox. Spat. Vis. 10, 443-446 (1997).
- D. G. Pelli, The VideoToolbox software for visual psychophysics: Transforming numbers into movies. Spat. Vis. 10, 437-442 (1997).
- J. R. Manning et al., A probabilistic approach to discovering dynamic full-brain functional connectivity patterns. NeuroImage 180, 243-252 (2018).
- M. Kumar et al., BrainIAK: The brain image analysis kit. Apert. Neuro. 1, 1–19 (2021).

 A. Schaefer et al., Local-global parcellation of the human cerebral cortex from intrinsic functional connectivity MRI. Cereb. Cortex 28, 3095–3114 (2018).
- E. M. Gordon et al., Generation and evaluation of a cortical area parcellation from resting-state
- correlations. *Cereb. Cortex* **26**, 288–303 (2016). S. M. Smith, A. Hyvaärinen, G. Varoquaux, K. L. Miller, C. F. Beckmann, Group-PCA for very large fMRI datasets. NeuroImage 101, 738-749 (2014).
- D. M. Blei, A. Y. Ng, M. I. Jordan, Latent dirichlet allocation. J. Mach. Learn. Res. 3, 993-1022 (2003).
- A. S. Fox, L. J. Chang, K. J. Gorgolewski, T. Yarkoni, Bridging psychology and genetics using large-scale spatial analysis of neuroimaging and neurogenetic data. bioRxiv [Preprint] (2014). https://doi.org/10.1101/012310 (Accessed 15 March 2023).
- S. Sul, B. Güroğlu, E. A. Crone, L. J. Chang, Medial prefrontal cortical thinning mediates shifts in other-regarding preferences during adolescence. Sci. Rep. 7, 8510 (2017).
- P. H. A. Chen, E. Jolly, J. H. Cheong, L. J. Chang, Intersubject representational similarity analysis reveals individual variations in affective experience when watching erotic movies. NeuroImage 216, 116851 (2020).
- L. L. W. Owen, J. R. Manning. GitHub. https://github.com/ContextLab/pca_paper. Deposited 26 December 2023